Local Atomic Structure and Discommensurations in the Charge Density Wave of $CeTe_3$

H. J. Kim,[1] C. D. Malliakas,[2] A. T. Tomić,[1] S. H. Tessmer,[1] M. G. Kanatzidis,[2] and S. J. L. Billinge[1,*]

[1]*Department of Physics and Astronomy, Michigan State University, East Lansing, Michigan 48824, USA*

[2]*Department of Chemistry, Michigan State University, East Lansing, Michigan 48824, USA*

(Received 15 February 2006; published 5 June 2006)

The local structure of $CeTe_3$ in the incommensurate charge density wave (IC-CDW) state has been obtained using atomic pair distribution function analysis of x-ray diffraction data. Local atomic distortions in the Te nets due to the CDW are larger than observed crystallographically, resulting in distinct short and long Te-Te bonds. Observation of different distortion amplitudes in the local and average structures is explained by the discommensurated nature of the CDW, since the pair distribution function is sensitive to the local displacements within the commensurate regions, whereas the crystallographic result averages over many discommensurated domains. The result is supported by STM data. This is the first quantitative local structural study within the commensurate domains in an IC-CDW system.

DOI: 10.1103/PhysRevLett.96.226401 PACS numbers: 71.45.Lr, 61.10.Nz, 61.44.Fw

Incommensurate charge density waves (IC-CDWs) are a fundamental property of low-dimensional metals [1] and also underlie the novel properties of correlated electron oxides such as cuprates in the pseudogap state [2–4] and manganites at high doping [5]. Knowing the nature of local atomic displacements (Peierls distortions) in the IC-CDWs is crucial to understanding such factors as electron-lattice coupling [6], yet this information is difficult to obtain quantitatively. Here we solve this problem by taking the novel approach of using a local structural method, the atomic pair distribution function (PDF) technique [7], to determine the local atomic displacements with high precision in the system $CeTe_3$. IC-CDWs, and the underlying atomic displacements, can be uniform incommensurate modulations or locally commensurate waves separated by narrow domain walls, known as discommensurations [8], where the phase of the wave changes rapidly. Here we show that the IC-CDW in $CeTe_3$ is discommensurated and obtain for the first time the quantitative local atomic displacements within the commensurate domains.

In the case of *incommensurate* CDWs, superlattice peaks observed crystallographically yield the average distorted structure. Except in the cases where the domains are periodically arranged, giving rise to satellite peaks [9], it is not possible to determine whether the underlying CDW is truly incommensurate or forms a discommensurated structure with commensurate regions separated by domain walls [8]. A number of techniques have been successful at differentiating between the truly incommensurate and discommensurated cases. The earliest verification of a discommensurated phase came from photoemission spectroscopy evidence that the Ta $4f$ states in $1T$-TaS_2 had the same splitting in the commensurate and nearly commensurate states [10]. Photoemission is a local probe and found distinct Ta environments rather than a broad continuum expected from a purely incommensurate state. Similarly, another local probe, nuclear magnetic resonance (NMR), found distinct Knight shifts for three Se sites in the incommensurate state of $2H$-$TaSe_2$, similar to the commensurate phase [11,12]. High resolution atomic imaging methods have also contributed to this debate. The strain fields due to the domain walls were observed in dark field transmission electron microscopy measurements [13]. Interestingly, atomic resolution images in real space have difficulty in resolving discommensurated domains [14–17]. However, Fourier analysis of scanning tunneling microscopy (STM) images can be a reliable measure, as discussed in detail by Thomson *et al.* [18].

As in the case of the NMR and photoemission studies, the PDF approach described here makes use of the fact that the local structure deviates from the average in the discommensurated case. By comparing atomic displacements determined from the PDF with those determined crystallographically, we establish the presence of commensurate domains but, crucially, also obtain quantitatively the atomic structure within these domains. This novel approach is applied here to the incommensurate phase of $CeTe_3$.

In its undistorted form, $CeTe_3$ takes the $NdTe_3$ structure type with space group *Cmcm* [19]. It forms a layered structure with ionic $[Ce_2^{3+}Te_2^{2-}]^{2+}$ layers sandwiched between two Te^- layers. These sandwich layers stack together with weak van der Waals forces to form the three-dimensional structure. Te ions in the Te^- layers form a square net with 3.1 Å Te-Te bonds. The structure is shown in Fig. 1(a). The electronic bands crossing the Fermi level are Te p bands from the 2D square nets [20], and the CDW forms in these metallic layers. In the CDW state, an incommensurate superlattice is observed [20,21], with a wave vector characteristic of a strong Fermi-surface nesting vector in the electronic structure [22–25]. This is a surprisingly stable and simple single-q IC-CDW state in an easily cleavable 2D square net, making the RTe_3 (R denotes rare earth metal) systems ideal for studying the IC-CDW state [20]. The atomic distortions giving rise to the superlattice have been solved crystallographically from

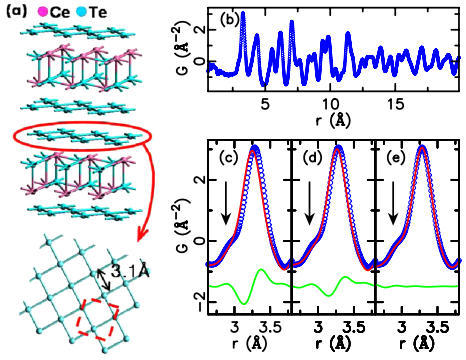

FIG. 1 (color online). (a) The crystal structure of $CeTe_3$ with the square Te net that supports the CDW highlighted. The reduced unit cell on the Te net is indicated by the red dashed box. (b) The PDF of $CeTe_3$ at room temperature. In (c)–(e), the first peak of the experimental PDF of $CeTe_3$ (blue circles) is plotted with the calculated PDF (red line) from various models: (c) the undistorted crystal structure model (*Cmcm*), (d) the distorted-crystallographic model, and (e) the local structural model determined from a PDF refinement over the range $2.5 < r < 6.37$ Å. The difference between the experimental and calculated PDFs (green line) is plotted below the data in each panel. The shoulder due to the Peierls distortions in the Te nets is indicated by an arrow.

single crystal x-ray diffraction data [21]. The incommensurate wavelength of the distortion is close to $25a/7$, where a is the lattice parameter of the undistorted phase. The distorted structure is in the *Ama2* space group [21]. From the crystallography alone, it is not possible to determine whether this distorted structure is truly incommensurate or whether discommensurations form between short-range commensurate domains.

The x-ray PDF experiment was conducted on a fine powder of $CeTe_3$ prepared as described in Ref. [21]. $CeTe_3$ powder was loosely packed in a flat plate with thickness of 1.0 mm sealed with kapton tape. Care must be taken when grinding this material or turbostratic disorder is introduced, significantly modifying the stacking of the layers. Diffraction data were collected at 300 K using the rapid acquisition pair distribution function technique [26]. Standard corrections [7,26] were made using the program PDFGETX2 [27] to obtain the properly normalized total scattering function $S(Q)$ [7], which was truncated at $Q_{\max}$ of 25 Å^{-1} before Fourier transforming to obtain the PDF $G(r) = \frac{2}{\pi}\int_0^\infty Q[S(Q) - 1]\sin(Qr)dQ$. Structural models are fit to the data using the program PDFFIT [28].

The PDF of $CeTe_3$, measured at room temperature, is shown in Fig. 1(b). The PDF gives the probability of finding an atom at a distance r away from another atom. The nearest neighbor peak around 3.1 Å comes from the Te-Te bond in the nets and the Ce-Te bond in the intergrowth layers. This is shown on an expanded scale in Figs. 1(c)–1(e). A shoulder is evident on the low-r side of the peak. This feature is robust; it is much larger than the statistical and systematic errors and is reproduced in measurements of isostructural compounds $NdTe_3$ and $PrTe_3$. Figure 1(c) shows the fit to this peak of the undistorted crystal structure model (*Cmcm*), where only symmetry allowed atomic positions and isotropic thermal factors were refined. The result clearly does not explain this shoulder which originates from short Te-Te bonds in the Te net. Surprisingly, however, the PDF calculated from the *distorted* structure determined crystallographically [21] also does not explain this shoulder well. In this case, the atoms were fixed at the crystallographically determined positions and isotropic thermal factors were refined. This resulted in a better fit to the first peak [Fig. 1(d)]; however, the fit is not ideal and required a large value of U_{iso} for the Te atoms in the nets [$U_{\text{iso}} = 0.0152(2)$ Å^2]. The value was 2 times larger than U_{iso} of the Ce and Te atoms in the ionic $[Ce_2^{3+}Te_2^{2-}]^{2+}$ layers [0.0077(2) and 0.0080(2) Å^2 for U_{iso} of Ce and Te atoms, respectively].

The large fluctuation in the difference curve in Fig. 1(c) arises because the real distribution of Te-Te bond lengths in the data is broader than in the undistorted model. This fluctuation in the difference curve is smaller in Fig. 1(d) because the distortions of the Te net in the *Ama2* crystallographic model result in a broader Te-Te bond-length distribution. However, clearly the distorted-crystallographic model still has a Te-Te bond-length distribution that is narrower than in the data. We therefore refined the Te-net distortions directly in the PDF by allowing the atomic positions in the model to vary. The model was constrained to have the *Ama2* symmetry, and the same unit cell was used as in the distorted-crystallographic model. The refinement result for $2.5 < r < 6.37$ Å is shown in Fig. 1(e). As well as giving a significantly better fit to the low-r region of the PDF, this refinement resulted in much smaller and more physical thermal factors on the planar Te ions.

The model of the local structure refined from the PDF gives a broader range of Te-Te bond lengths (from 2.83 to 3.36 Å) than the crystallographic distorted model (from 2.94 to 3.26 Å). It is also interesting to see the shape of the bond-length *distributions* for the Te-Te bonds in the Te nets from these two models. These are shown in Fig. 2. The dark (blue) solid line shows the bond-length distribution refined from the PDF, and the light (red) line is the distribution from the crystallographic model [21]. For direct comparison, the distributions are plotted using the same thermal broadening of 0.007 Å^2. The distorted-crystallographic model has broad but symmetric and Gaussian bond-length distribution coming from the continuous distribution of Te-Te bond lengths in the *average* IC-CDW. On the other hand, the local structure refinement ($r_{\max} = 6.37$ Å) yields a bond-length distribution that is clearly bimodal and is separated into distinct "short" and "long" Te-Te distances. This is emphasized in Fig. 2(b), where we show a fit of two, well separated, Gaussian curves to the PDF-refined bond-length distribution. This behavior is charac-

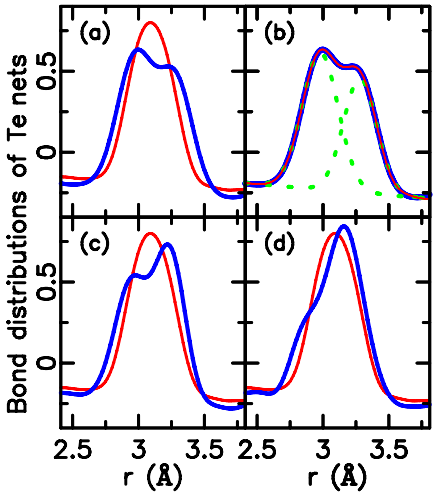

FIG. 2 (color online). Bond-length distributions in the Te nets refined from the PDF over various r ranges [dark (blue) line]: (a) $r_{max} = 6.37$ Å, (b) $r_{max} = 6.37$ Å, (c) $r_{max} = 14.5$ Å, (d) $r_{max} = 27.1$ Å. The r_{min} value was fixed to 2.5 Å for all the cases. The bond distribution from the distorted-crystallographic model [light (red) line] is plotted in (a), (c), and (d) for comparison. In (b), the bond distribution of the local structural model ($r_{max} = 6.37$ Å) is fit with two Gaussians. The fit is shown as a light (red) line and the two Gaussian subcomponents as a dotted (green) line.

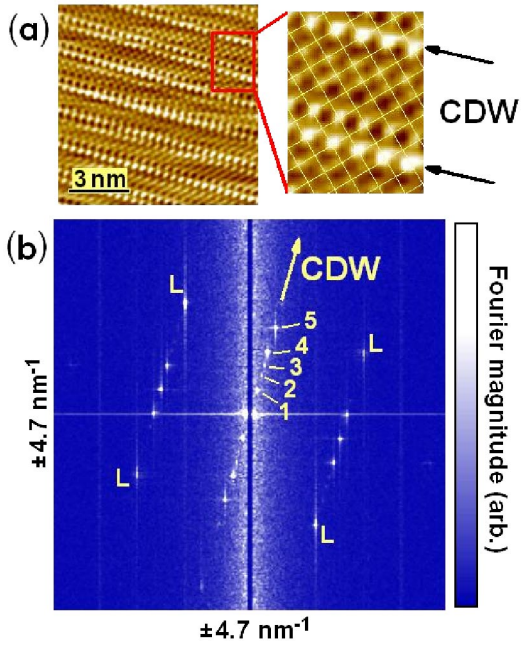

FIG. 3 (color online). (a) A representative STM image from the Te net showing the CDW. On the expanded image, the network of Te bonds is superimposed. (b) The Fourier transform of the STM data. To achieve a high signal-to-noise ratio, the transform represents the average of 24 images (each image was 27×27 nm). The unprocessed transform image shows enhanced noise along the vertical axis, an artifact due to the scan direction. This noise was removed to better resolve the peaks near the origin. The square Te net gives rise to four distinct peaks (L), with peaks related to the CDW oriented at 45°, as indicated by the arrow. The fundamental CDW peak (corresponding to a wavelength of ≈ 15 Å) and the $\lambda/2$ harmonic are labeled 1 and 3, respectively. Peaks 2 and 4 are in close proximity to 3, implying a characteristic discommensuration length of 38 Å, as described in the text. Peak 5 corresponds to the diagonal of the Te net. This component may be enhanced due to the underlying crystal structure; the CDW-lattice interaction may also enhance this peak.

teristic of oligomerization with Te forming bonded and nonbonded interactions with its neighbors in the net [29] that would be expected in a commensurate structure. Since we know that the modulation is incommensurate on average, this is strong evidence that the structure consists of commensurate domains separated by discommensurations. As r_{max} in the PDF refinements is increased, the PDF-refined distribution crosses over towards the crystallographic result and by $r_{max} = 27.1$ Å, resembles it rather closely [Fig. 2(d)].

We have applied STM on the exposed Te net of a cleaved single crystal of $CeTe_3$, grown according to the method described in Ref. [21]. Measurements were done at 300 K in the constant current mode of the STM. Data were acquired with a bias voltage of 100 mV and with a tunneling current of 0.6 nA. Figure 3(a) shows a representative atomic resolution image with the CDW modulation clearly visible oriented at 45° to the net. To investigate the images for discommensurations, we examine the corresponding two-dimensional Fourier transform, shown in Fig. 3(b). As indicated by the labels, in addition to the fundamental CDW peak (1), four more peaks lie along the CDW direction (2)–(5). Although the transforms of real-space images resemble diffraction data, symmetry requirements intrinsic to diffraction data do not apply. As demonstrated by Thomson and co-workers, the Fourier transforms of STM images that exhibit true discommensurations always have extra peaks in proximity to the fundamental CDW peak [18]. This arises from the fact that a discommensurate CDW can be expressed as the product of a uniformly incommensurate CDW and a modulation envelope [18]. The wavelengths of the envelope are given by the differences in the wave vectors of closely spaced peaks. The longest such wavelength in our images is 38 Å, corresponding to peaks 2–3 and 3–4 in the Fourier transform, indicating that a discommensuration separation of this length scale exists. This is consistent with the refined PDF behavior, which crosses over from the local to the average behavior for a refinement range of around 27 Å (Fig. 2), which would be expected to occur at around, or a little above, the *radius* of the local domains.

As well as the bond-length distributions, the local and average structure refinements allow us to study the patterns of atomic displacements due to the IC-CDW. The average structure refinement [21] results in an almost perfectly

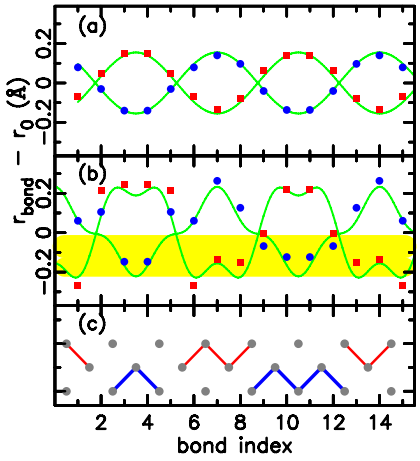

FIG. 4 (color online). Te-Te bond-length deviation from the average value as refined (a) crystallographically and (b) from the PDF. The deviation $r_{\text{bond}} - r_0$ is defined such that r_i is the Te-Te bond length of the ith bond (bond index i) in the unit cell and $r_0 = 3.1$ Å. (c) Schematic of the arrangements of short Te-Te bonds within the unit cell coming from the PDF refinements and highlighting the formation of oligomers. Light (dark) lines and square (circular) markers are "short bonds" lying in the top (bottom) row of the unit cell. Short bonds are defined as those whose length lies within the shaded (yellow) band in (b). This shaded (yellow) band is centered at the position of the *first* Gaussian of the bimodal distribution in Fig. 2(b) and has a width of one standard deviation of that Gaussian.

sinusoidal pattern of bond lengths, with the wavelength of the CDW [Fig. 4(a)], clearly identifying these as Peierls distortions. The local structural model was refined in the same unit cell and space group but results in a much more square-wave-like distribution, consistent with the distinct short and long Te-Te distances described above [Fig. 4(b)]. Figure 4(c) shows the pattern of Te-Te short bonds, as defined in the figure caption, that results when the short distances determined from the PDF data are plotted in the unit cell. In this way, the Peierls distortions are seen to result in oligomers, or short segments of bonded Te atoms, in the Te net. In this picture, the discommensurations occur when the pattern of oligomers has defects. This is a common picture in the chemistry literature [21,30], though we note that this picture is not supported by the crystallographic results shown in Fig. 4(a) and needed the application of a local structural method to show that it has a physical reality beyond its heuristic value.

The refined parameters of the low-r_{max} PDF refinements yield quantitatively the atomic displacements within the commensurate domains. This is the first demonstration of the use of the PDF to obtain quantitatively the atomic displacements (Peierls distortion) within the commensurate domains of a discommensurated IC-CDW. This opens the way to a quantitative first-principles calculations and a better microscopic understanding of the IC-CDW state.

We gratefully acknowledge P. M. Duxbury, S. D. Mahanti, and D. I. Bilc for discussions and D. Robinson and D. Wermeille for help with collecting data. Work was supported by the National Science Foundation through Grants No. DMR-0304391, No. DMR-0443785, and No. DMR-0305461. MUCAT is supported by the U.S. Department of Energy through Contract No. W-7405-Eng-82 and the APS by Contract No. W-31-109-Eng-38.

*Electronic address: billinge@pa.msu.edu

[1] G. Grüner, *Density Waves in Solids* (Addison-Wesley, New York, 1994).
[2] M. Vershinin *et al.*, Science **303**, 1995 (2004).
[3] J. E. Hoffman *et al.*, Science **295**, 466 (2002).
[4] T. Hanaguri *et al.*, Nature (London) **430**, 1001 (2004).
[5] J. C. Loudon *et al.*, Phys. Rev. Lett. **94**, 097202 (2005).
[6] G. C. Milward, M. J. Calderón, and P. B. Littlewood, Nature (London) **433**, 607 (2005).
[7] T. Egami and S. J. L. Billinge, *Underneath the Bragg Peaks: Structural Analysis of Complex Materials* (Pergamon, Oxford, England, 2003).
[8] W. L. McMillan, Phys. Rev. B **14**, 1496 (1976).
[9] D. E. Moncton, J. D. Axe, and F. J. DiSalvo, Phys. Rev. B **16**, 801 (1977).
[10] H. P. Hughes and R. A. Pollack, Commun. Phys. **1**, 61 (1976).
[11] B. H. Suits, S. Couturie, and C. P. Slichter, Phys. Rev. Lett. **45**, 194 (1980).
[12] B. H. Suits, S. Couturie, and C. P. Slichter, Phys. Rev. B **23**, 5142 (1981).
[13] C. H. Chen, J. M. Gibson, and R. M. Fleming, Phys. Rev. Lett. **47**, 723 (1981).
[14] J. M. Gibson, C. H. Chen, and M. L. McDonald, Phys. Rev. Lett. **50**, 1403 (1983).
[15] T. Ishiguro and H. Sato, Phys. Rev. B **44**, 2046 (1991).
[16] M. Kuwabara *et al.*, Phys. Status Solidi A **96**, 39 (1986).
[17] J. W. Steeds *et al.*, Ultramicroscopy **18**, 97 (1985).
[18] R. E. Thomson *et al.*, Phys. Rev. B **49**, 16 899 (1994).
[19] W. Lin, H. Steinfink, and E. J. Weiss, Inorg. Chem. **4**, 877 (1965).
[20] E. DiMasi *et al.*, Phys. Rev. B **52**, 14 516 (1995).
[21] C. Malliakas *et al.*, J. Am. Chem. Soc. **127**, 6510 (2005).
[22] G. H. Gweon *et al.*, Phys. Rev. Lett. **81**, 886 (1998).
[23] V. Brouet *et al.*, Phys. Rev. Lett. **93**, 126405 (2004).
[24] H. Komoda *et al.*, Phys. Rev. B **70**, 195101 (2004).
[25] J. Laverock *et al.*, Phys. Rev. B **71**, 085114 (2005).
[26] P. J. Chupas *et al.*, J. Appl. Crystallogr. **36**, 1342 (2003).
[27] X. Qiu, J. W. Thompson, and S. J. L. Billinge, J. Appl. Crystallogr. **37**, 678 (2004).
[28] T. Proffen and S. J. L. Billinge, J. Appl. Crystallogr. **32**, 572 (1999).
[29] R. Patschke and M. G. Kanatzidis, Phys. Chem. Chem. Phys. **4**, 3266 (2002).
[30] R. Patschke *et al.*, J. Am. Chem. Soc. **123**, 4755 (2001).